GW190425: Pan-STARRS and ATLAS coverage of the skymap and limits on optical emission associated with FRB 20190425A

Monthly Notices of the ROYAL ASTRONOMICAL SOCIETY

MNRAS **528,** 2299–2307 (2024) https://doi.org/10.1093/mnras/stae100
Advance Access publication 2024 January 12

GW190425: Pan-STARRS and ATLAS coverage of the skymap and limits on optical emission associated with FRB 20190425A

S. J. Smartt [1,2★] M. Nicholl [2] S. Srivastav [2] M. E. Huber [3] K. C. Chambers [3] K. W. Smith [2] D. R. Young [2] M. D. Fulton [2] J. L. Tonry [3] C. W. Stubbs [4] L. Denneau,[3] A. J. Cooper [1] A. Aamer [2] J. P. Anderson [5,6] A. Andersson [1] J. Bulger,[3] T.-W. Chen [7] P. Clark [8] T. de Boer,[3] H. Gao [3] J. H. Gillanders [1] A. Lawrence [3] C. C. Lin [3] T. B. Lowe,[3] E. A. Magnier [3] P. Minguez,[3] T. Moore [2] A. Rest [9,10] L. Shingles [11] R. Siverd [3] I. A. Smith [12] B. Stalder [13] H. F. Stevance [1] R. Wainscoat [3] and R. Williams[14]

[1]*Astrophysics Sub-department, Department of Physics, University of Oxford, Keble Road, Oxford OX1 3RH, UK*
[2]*Astrophysics Research Centre, School of Mathematics and Physics, Queen's University Belfast, Belfast, BT7 1NN, UK*
[3]*Institute for Astronomy, University of Hawai'i, 2680 Woodlawn Drive, Honolulu, HI 96822, USA*
[4]*Department of Physics and Department of Astronomy, Harvard University, Cambridge, MA 02138, USA*
[5]*European Southern Observatory, Alonso de Córdova 3107, Casilla 19, Santiago, Chile*
[6]*Millennium Institute of Astrophysics (MAS), Nuncio Monseñor Sótero Sanz 100, Off. 104, Providencia, Santiago, Chile*
[7]*Graduate Institute of Astronomy, National Central University, 300 Jhongda Road, 32001 Jhongli, Taiwan*
[8]*Institute of Cosmology and Gravitation, University of Portsmouth, Portsmouth PO1 3FX, UK*
[9]*Space Telescope Science Institute, 3700 San Martin Drive, Baltimore, MD 21218, USA*
[10]*Department of Physics and Astronomy, Johns Hopkins University, Baltimore, MD 21218, USA*
[11]*GSI Helmholtzzentrum für Schwerionenforschung, Planckstrasse 1, D-64291 Darmstadt, Germany*
[12]*Institute for Astronomy, University of Hawai'i, 34 Ohia Ku Street, Pukalani, HI 96768-8288, USA*
[13]*Vera C. Rubin Observatory Project Office, 950 N Cherry Ave, Tucson, AZ 95719, USA*
[14]*Institute for Astronomy, University of Edinburgh, Royal Observatory, Edinburgh, Blackford Hill, EH9 3HJ, UK*

Accepted 2024 January 4. Received 2024 January 2; in original form 2023 September 20

ABSTRACT

GW190425 is the second of two binary neutron star (BNS) merger events to be significantly detected by the Laser Interferometer Gravitational Wave (GW) Observatory (LIGO), Virgo and the Kamioka Gravitational Wave (KAGRA) detector network. With a detection only in LIGO Livingston, the skymap containing the source was large and no plausible electromagnetic counterpart was found in real-time searching in 2019. Here, we summarize Asteroid Terrestrial-Impact Last Alert System (ATLAS) and Panoramic Survey Telescope and Rapid Response System (Pan-STARRS) wide-field optical coverage of the skymap beginning within 1 and 3 h, respectively, of the GW190425 merger time. More recently, a potential coincidence between GW190425 and a fast radio burst FRB 20190425A has been suggested, given their spatial and temporal coincidences. The smaller sky localization area of FRB 20190425A and its dispersion measure led to the identification of a likely host galaxy, UGC 10667 at a distance of 141 ± 10 Mpc. Our optical imaging covered the galaxy 6.0 h after GW190425 was detected and 3.5 h after the FRB 20190425A. No optical emission was detected and further imaging at +1.2 and +13.2 d also revealed no emission. If the FRB 20190425A and GW190425 association were real, we highlight our limits on kilonova emission from a BNS merger in UGC 10667. The model for producing FRB 20190425A from a BNS merger involves a supramassive magnetized neutron star spinning down by dipole emission on the time-scale of hours. We show that magnetar-enhanced kilonova emission is ruled out by optical upper limits. The lack of detected optical emission from a kilonova in UGC 10667 disfavours, but does not disprove, the FRB–GW link for this source.

Key words: surveys – transients: neutron star mergers – transients: fast radio bursts – gravitational waves.

1 INTRODUCTION

The historic gravitational wave (GW) event GW170817 resulting from a binary neutron star (BNS) merger (Abbott et al. 2017a) produced a short gamma-ray burst (GRB170817A; Abbott et al. 2017c) and a rapidly evolving optical and infrared transient (AT2017gfo;

★ E-mail: stephen.smartt@physics.ox.ac.uk

Abbott et al. 2017b). The relatively small sky localization map (31 deg^2), inferred from the strong signals in the two (Laser Interferometer Gravitational Wave Observatory) LIGO detectors and an upper limit in Virgo (Abbott et al. 2017a), allowed the rapid identification of an optical counterpart. This was achieved 11 h after the BNS merger, during the first night of observing the skymap from Chile (Arcavi et al. 2017; Coulter et al. 2017; Lipunov et al. 2017; Soares-Santos et al. 2017; Tanvir et al. 2017; Valenti et al. 2017). Global monitoring followed, with the spectra from Chilean and South African observatories showing an unprecedented evolution within the first 24 h and confirming that this was the signature of a unique transient with no known counterpart (Chornock et al. 2017; McCully et al. 2017; Nicholl et al. 2017; Pian et al. 2017; Shappee et al. 2017; Smartt et al. 2017). The light-curve monitoring showed that AT2017gfo faded rapidly with the flux emission shifting to near-infrared and possibly even beyond (Andreoni et al. 2017; Cowperthwaite et al. 2017; Drout et al. 2017; Evans et al. 2017; Kasliwal et al. 2017; Kilpatrick et al. 2017; Tanvir et al. 2017; Troja et al. 2017; Utsumi et al. 2017). The transient was detected in the X-ray and radio a few days after the merger (Alexander et al. 2017; Haggard et al. 2017; Hallinan et al. 2017; Margutti et al. 2017; Troja et al. 2017), providing constraints on the jet physics giving rise to the short GRB.

GW170817 was discovered towards the end of the LIGO–Virgo collaboration's second observing run (O2) and at the time of writing (6 months into O4) only one further BNS merger has been detected and confirmed as a real signal (Abbott et al. 2021). GW190425 was observed in only one LIGO detector (Abbott et al. 2020) close to the start of the LIGO-Virgo - Kamioka Gravitational Wave detector (KAGRA) collaboration's third observing run (O3). With a signal only from Livingston, the sky localization map was very large and half of the high-probability region was in the daytime sky. No electromagnetic counterpart was discovered at the time at any wavelength (Coughlin et al. 2019; Smith et al. 2019b; Boersma et al. 2021; Paterson et al. 2021), which was not a major surprise given the large skymap, the inferred distance $D_L = 159^{+69}_{-72}$ Mpc (from the GW analysis of Abbott et al. 2020), and solar conjunction.

Fast radio bursts (FRBs) are extragalactic millisecond-duration bursts of unknown origin. The large all-sky rate of FRBs appears inconsistent with a single compact object merger origin of all sources (Ravi 2019). However, some models suggest that mergers may be responsible for a subset of FRBs, powered by either pre-merger magnetic interaction (e.g. Totani 2013) or the merger remnant (e.g. Falcke & Rezzolla 2014). These models can be effectively tested by performing prompt FRB searches on localization regions of GW events and short GRBs, or through post-FRB follow-up observations of nearby sources in search of a kilonova or radio afterglow (Cooper et al. 2023).

A search for spatial and temporal coincidences of GW events and FRBs by Moroianu et al. (2023) proposed a link between FRB 20190425A and GW190425. They searched for GW–FRB coincidences with the Canadian Hydrogen Intensity Mapping Experiment FRB (CHIME/FRB) catalogue (CHIME/FRB Collaboration 2021) and the O3 Gravitational Wave Transient Catalogue number 2 (GWTC-2) catalogue (Abbott et al. 2021). They used a time window of 26 h, from 2 h before the GW event and up to 24 h after. The CHIME sky localization region is typically of the order of arcminutes in diameter, much smaller than that of GW sources (tens to hundreds of deg^2 depending on the number of detectors retrieving a signal).

FRB 20190425A was detected at MJD 58598.44899 (2019 April 25 10:46:33 UT; CHIME/FRB Collaboration 2021), which was 2.5 h after GW190425 (Moroianu et al. 2023). Moroianu et al. (2023) report that its estimated sky position of RA $= 255.72 \pm 0.14^\circ$ and Dec. $= 21.52 \pm 0.18^\circ$ places it within the 66.7 per cent probability contour of the final, most reliable skymap from GWTC-2 (Abbott et al. 2021). In addition, the dispersion measure (DM) of FRB 20190425A provides an upper limit to the redshift of $z < 0.0394$ corresponding to a luminosity distance[1] of $D_L < 179$ Mpc. The FRB and GW signals were therefore coincident in their sky positions, distances, and time (given the definition of coincidences described). Moroianu et al. (2023) propose that there is only one catalogued galaxy (in NED, the NASA/Infrared Processing and Analysis Centre Extragalactic Database) within the CHIME error ellipse that has a measured spectroscopic redshift placing it within the upper limit measured from the DM of $z < 0.0394$. This is UGC 10667, at a redshift of $0.031\,224 \pm 0.000\,011$ (Albareti et al. 2017, from Sloan Digital Sky Survey, SDSS Data Release 13). We adopt a foreground extinction towards UGC 10667 of $E(B-V) = 0.066$, corresponding to $A_g = 0.247$, $A_r = 0.171$, and $A_i = 0.127$ (Schlafly & Finkbeiner 2011).

Panther et al. (2023) further investigated the plausibility of UGC 10667 being the host of FRB 20190425A with a different method. Moroianu et al. (2023) considered the optimal 68 per cent localization ellipse of FRB 20190425A from CHIME, with dimensions $0.1^\circ \times 0.2^\circ$. Panther et al. (2023) went further and employed the full CHIME localization contours to produce a ranked list of all galaxies (ranked by probability of association) within $z < 0.06$ using the Probabilistic Association of Transients to their Hosts (PATH) formalism of Aggarwal et al. (2021). Both papers favour this galaxy as the host.[2] The redshift corresponds to a Hubble flow distance of $D_L = 141 \pm 10$ Mpc (corrected for Virgo infall, from NED), consistent with the LIGO–Virgo–KAGRA distance constraint $D_L = 159^{+69}_{-72}$ Mpc (Abbott et al. 2020) and the upper limit to the FRB DM $D_L < 179$ Mpc. Panther et al. (2023) find that UGC10667 is a spiral galaxy with a modest star formation rate and luminosity dominated by an old stellar population. They also searched for transient radio emission in and around the galaxy at 2.5 yr post-burst that could be associated with either the FRB 20190425A or GW190425 and found no convincing radio transient emission in Very Large Array 6 Ghz data taken in 2021 September and October.

Moroianu et al. (2023) and Panther et al. (2023) highlight that FRB 20190425A had a number of notable properties: one of lowest DM non-repeating events in the CHIME/FRB Catalogue 1, a high flux for those with low DMs, a short pulse duration, and a flat spectrum. All of this led Moroianu et al. (2023) to suggest that the co-production of GW190425 and FRB 20190425A could be explained by the theory of Zhang (2014). In this scenario, the BNS merger produces a supramassive neutron star (NS), which is highly magnetized. The compact object has a short rotation period and loses angular momentum as it spins down and collapses to a black hole. The FRB is created as the magnetosphere is ejected (Falcke & Rezzolla 2014), through the so-called blitzar mechanism. The supramassive NS must survive for 2.5 h, the time between merger and the FRB. While the data and theory of association are intriguing, Bhardwaj et al. (2023a) have cautioned against assuming physical association from analysis of the GW signal and constraints on the ejecta mass for the 400 MHz radio signal to propagate. Furthermore, Abbott

[1]We assume a standard flat cosmology with $H_0 = 68$ km s^{-1} Mpc^{-1} from the Planck Collaboration XIII (2016) as adopted in Abbott et al. (2020).
[2]While this paper was being refereed, Bhardwaj et al. (2023b) used the CHIME baseband data to confirm UGC 10667 as the likely host of FRB 20190425A.

et al. (2023) performed a search for GW transients associated with 40 CHIME FRBs during the O3a run. No significant evidence was found for GW emission at the time of any of the FRBs within a narrow 12 s window.

In this paper, we present a summary of the Asteroid Terrestrial-Impact Last Alert System (ATLAS) and Panoramic Survey Telescope and Rapid Response Syste, or Pan-STARRS (PS), wide-field optical coverage of the GW190425 skymap starting 0.8 and 1.36 h, respectively, after the BNS merger.We present images of the proposed most likely host of FRB 20190425A (UGC 10667) taken over the first few nights, finding no optical transient emission. We also report publicly available Zwicky Transient Facility (ZTF) data (Bellm et al. 2019) of the host. We discuss the plausibility of the GW–FRB link assuming that the host galaxy is indeed UGC 10667 and the BNS produced a kilonova through mass ejection.

2 OBSERVATIONS AND DATA

2.1 Pan-STARRS1 observations and data

The PS is a dual 1.8 m telescope system (PS1 and PS2) each equipped with a 1.4 Gigapixel camera located at the summit of Haleakala on the Hawaiian island of Maui (Chambers et al. 2016). The data for this paper were all taken with the PS1 telescope and camera. The 0.26 arcsec pixels give a focal plane of 3.0° diameter, which corresponds to a field-of-view area of 7.06 deg^2. It is equipped with a filter system, denoted as $grizy_{\rm P1}$ as described in Tonry et al. (2012). The Pan-STARRS1 Science Consortium 3π Survey produced $grizy_{\rm P1}$ images of the whole sky north of $\delta = -30°$ (Chambers et al. 2016). We also have proprietary $i_{\rm P1}$ data in the range $-40° < \delta < -30°$. These data provide reference images for immediate sky subtraction. Images from PS1 are processed immediately with the Image Processing Pipeline (Magnier et al. 2020a; Waters et al. 2020).

The individual exposure frames (called warps) are astrometrically and photometrically calibrated (Magnier et al. 2020c). The 60 CCDs in Gigapixel Camera-1 (GPC1) are processed individually and warped on to a fixed tessellation of skycells as described in Chambers et al. (2016), each of which is typically 24 arcmin × 24 arcmin.Overlapping exposures can be co-added together (on the skycell tessellation) with median clipping applied (to produce nightly stacks). The PS1 3π reference sky images are subtracted from both the warps and the stacks (Waters et al. 2020) and photometry carried out on the resulting difference image (Magnier et al. 2020b). These individual detections are ingested into the Pan-STARRS Transient Server data base at Queen's University Belfast and assimilated into distinct objects with a time variable history. A series of quality filters are applied using the Image Processing Pipeline (IPP) image attributes and known asteroids and variable stars are removed. The objects remaining are cross-matched with all catalogued galaxies, active galactic nuclei (AGNs), Cataclysmic Variables (CVs), and historical transients (Smartt et al. 2016a) and simultaneously a machine learning algorithm is applied to image pixel stamps at each transient position (Wright et al. 2015). This reduces the bogus detections to a manageable number for human scanning. During the first three LIGO–Virgo and LIGO–Virgo–KAGRA observing runs, we had a programme in place to cover the GW skymaps for optical/near-infrared counterpart searches (Smartt et al. 2016a, b) and can typically cover 500–1000 deg^2 per night multiple times with one PS telescope. At the time of GW190425, we were using PS1 as the primary search facility for optical counterparts to GW sources.

GW190425 was discovered at MJD = 58598.34589 or 2019 April 25 08:18:05 UT (data from LIGO Scientific Collaboration & The Virgo Collaboration 2019b), and announced publicly with an initial localization skymap in a Gamma-ray Coordination Network (GCN) circular 95 min later at MJD = 58598.4118 (LIGO Scientific Collaboration & The Virgo Collaboration 2019a). We began observing the initial LIGO–Virgo–KAGRA `bayestar.fits` skymap (Singer & Price 2016) with PS1 beginning at MJD = 58598.40265, or 1.36 h after the BNS merger time. A series of dithered and overlapping 45 s exposures were taken in the *i* band over a period of 2 h. The images were typically taken in a set of 4 × 45 s, separated across 1 h or so to identify and remove moving objects. The images can either be processed individually or co-added to create a single stacked image for each PS skycell (Chambers et al. 2016). Standard processing as described above was immediately carried out on all the individual 45 s exposures and these had typical limiting magnitudes of $i_{\rm P1} > 21.3 \pm 0.3$ AB. These values represent the median of the 3.5σ upper limits of the processed skycells and the standard deviation of the sample. While we used the `bayestar.fits` skymap to define our pointings at the time of the event, an updated map is available from the GWTC-2 release (Abbott et al. 2021) and all probability sky coverage in this paper is with respect to that map (`gw190425z_skymap.multiorder.fits`).[3]

On this first night, we covered 1266 deg^2 of the GWTC-2 skymap, which corresponds to a cumulative probability coverage of 23.8 per cent. This was incremented over the first 3 d to cover 1374 deg^2 (24.9 per cent). At the time, we released 25 transients detected in the skymap (Smith et al. 2019b, c) but none of these emerged as a compelling candidate for an optical counterpart of GW190425 lying in a host galaxy within the GW-constrained redshift range. A number of candidates were followed up, and PS19qp showed a red continuum (Jonker et al. 2019; Nicholl et al. 2019b) but it was subsequently classified as a Type Ic supernova suffering significant extinction (Dimitriadis et al. 2019; McCully et al. 2019; Morokuma et al. 2019). Fig. 1 shows the PS1 skymap coverage over the first 3 d.

In the context of FRB 20190425A and its most likely host galaxy UGC 10667 (RA = 255.662 479 and Dec. = 21.576 746), we covered the position of this galaxy with PS1 within a few hours of both the FRB and the GW signals. A single 45 s $i_{\rm P1}$-band image was taken at 58598.5957604, which is 6.0 h after GW190425 merger time. The image is of good quality, taken at an airmass of 1.04 and with image's full width at half-maximum of 0.97 arcsec. The image is shown in Fig. 4 along with the PS1 3π reference image (Chambers et al. 2016) and the difference image created from subtracting the latter from the target image. There is no transient source visible in the PS1 images either in or around UGC 10667. There is a residual at the core of the galaxy that is almost certainly an image subtraction artefact and this is visible in historic monitoring of this sky region. We estimate a 3.5σ limit in the skycell of the image containing UGC 10667 to be $i > 21.6$. The limit is estimated using the method described in Magnier et al. (2020b), in which the flux and variance images are smoothed with a circularly symmetric Gaussian kernel and a significance image in signal-to-noise units is generated. A manual check of the background sky noise in a point spread function aperture and locating the faintest sources detected and visible in the image yields a detection limit of $i_{\rm P1} > 21.5$–21.8, corroborating the PS1 processing method. The circular radius around the core of UGC 10667 that contains good and complete pixel data is 32.0 arcsec, or a projected galactocentric distance in the sky plane of the galaxy of $R_{\rm g} = 20.5$ kpc. Therefore, we can say with reasonable confidence that there is no optical transient

[3] `gw190425z_skymap.multiorder.fits` is available on https://gracedb.ligo.org/superevents/S190425z/view/.

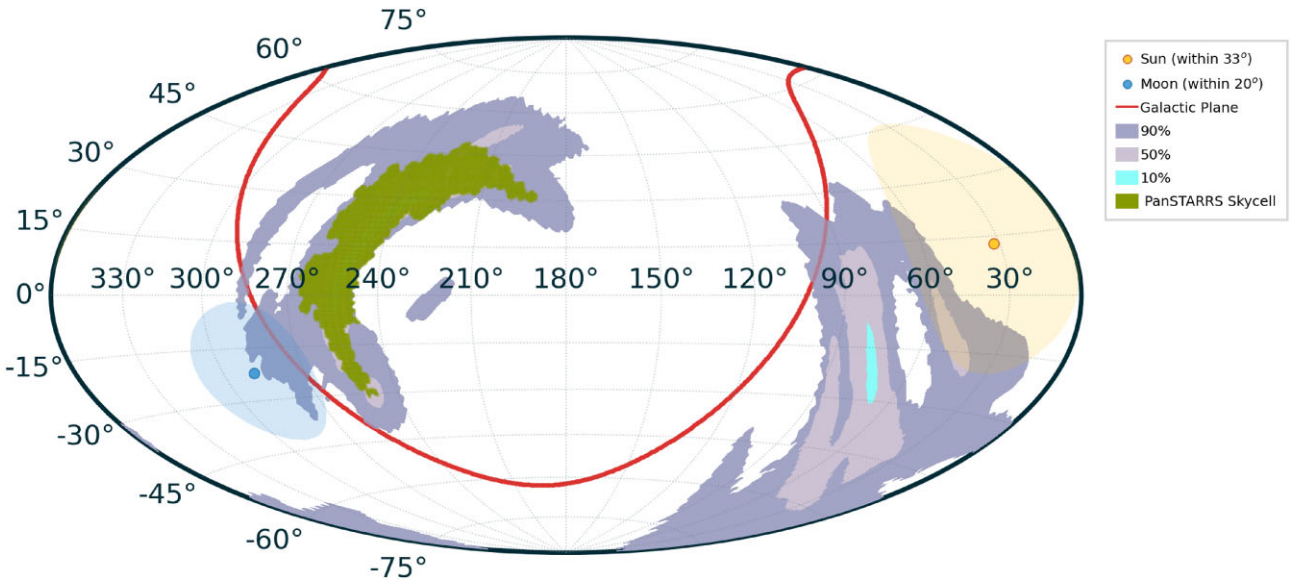

Figure 1. The PS1 coverage over the first three nights of observation starting 1.36 h after the detection of GW190425. We used the `bayestar.fits` skymap to define our pointings at the time, but the map above shows the final GWTC-2 skymap as released on GraceDB. The cumulative probability covered after one night was 23.8 per cent, which was incremented to 24.9 per cent after three nights.

Table 1. The 3.5σ limits of the PS1, ATLAS, and ZTF images of UGC 10667 around the time of GW190425. The epoch refers to the time of the image compared to the merger time of GW190425, in units of days.

MJD	Epoch	Telescope	ExpTime (s)	Filter	Limit
58598.414317	+0.067 75	ZTF	30	g	>20.6
58598.445932	+0.099 36	ZTF	60	r	>21.0
58598.595760	+0.249 19	PS1	45	$i_{\rm P1}$	>21.6
58598.635555	+0.288 99	ATLAS	30	o	>18.2
58599.254896	+0.908 33	ZTF	90	g	>21.3
58599.396968	+1.050 40	ZTF	90	r	>20.4
58599.576363	+1.229 79	ATLAS	120	o	>20.6
58600.392824	+2.046 25	ZTF	30	g	>21.1
58611.567044	+13.220 47	PS1	180	$w_{\rm P1}$	>23.4
58633.524370	+35.177 80	PS1	180	$w_{\rm P1}$	>22.6

within 20.5 kpc of UGC 10667 to a limiting magnitude of $i_{\rm P1} > 21.6$, at 6 h after GW190425 merger time. We revisited this sky region +13.2 and +35.2 d later during routine PS1 sky survey operations. A quad of images was taken on each occasion (4 × 45 s), in the $w_{\rm P1}$ filter and these were combined to create a nightly stack (a 180 s exposure). No transient source was detected in the difference images to $w_{\rm P1} >$ 23.5 and $w_{\rm P1} > 22.6$ on either night, respectively. A summary of the limiting magnitudes is listed in Table 1. Although a projected offset of 20 kpc would enclose most short GRBs (Fong et al. 2022) and the few candidate kilonovae known, the recent GRB230307A and its associated kilonova were observed at an offset of 40 kpc from its likely host (Gillanders et al. 2023; Levan et al. 2023; Yang et al. 2023). The ATLAS data described in Section 2.2 do not suffer from this pixel chip gap issue.

Panther et al. (2023) highlight six other galaxies that they estimate had a non-zero probability of being the candidate host of FRB 20190425A, in their methodology. The probabilities of any of them being the host ranged from 1 to 3.3 per cent (table 1 in Panther et al. 2023). We covered all apart from WISEAJ170930.73+213633.8 with PS1 imaging on the first night and no positive and significant transient sources were detected in the difference images. No automated detections were found and all images were inspected visually. WISEAJ170930.73+213633.8 (probability of being the host of FRB 20190425A, $P_{\rm PATH} = 0.0311$) fell on a chip gap and no definitive conclusion on transient emission can be drawn.

2.2 ATLAS observations and data

At the time of writing, ATLAS is operating as a four-telescope survey system with identical units in Haleakala and Mauna Loa (in Hawaii), El Sauce (Chile), and Sutherland (South Africa). However, during the O3 observing run, the two operational telescopes were the northern units. As described in Tonry et al. (2018), each ATLAS unit is a 'Wright Schmidt'-type telescope with a 0.65 m primary and a Schmidt corrector providing a 0.5 m clear aperture. The detectors are STA-1600 CCDs, which are arrays of 10560 × 10560 9 µm pixels. The pixel scale of 1.89 arcsec gives a field of view of 28.9 deg^2 for each camera. In normal survey mode in 2019, we were typically covering the sky north of $\delta > -45^\circ$ every two nights. During the O2 and O3 observing runs, we frequently adjusted the ATLAS survey schedule to promptly cover GW maps, with no loss to the primary near-Earth asteroid mission. We discovered the fast transient ATLAS17aeu, which turned out to be a GRB afterglow, coincidentally in the skymap of the binary black hole merger GW170104 (Stalder et al. 2017)

After the GW190425 alert, we scheduled sequences of 30 s images in the ATLAS o band, and at each pointing position a sequence of quads (4 × 30 s) was taken. A summary of our observations was posted by McBrien et al. (2019). The images were processed with the ATLAS pipeline and reference images subtracted from each one (Tonry et al. 2018). Transient candidates were run through our standard filtering procedures within the ATLAS Transient Science server (Smith et al. 2020). After quality control filters and real-bogus labelling with machine learning algorithms, candidates were spatially cross-matched with known minor planets, and star, galaxy, AGN, and multiwavelength catalogues. We began observing the northern part

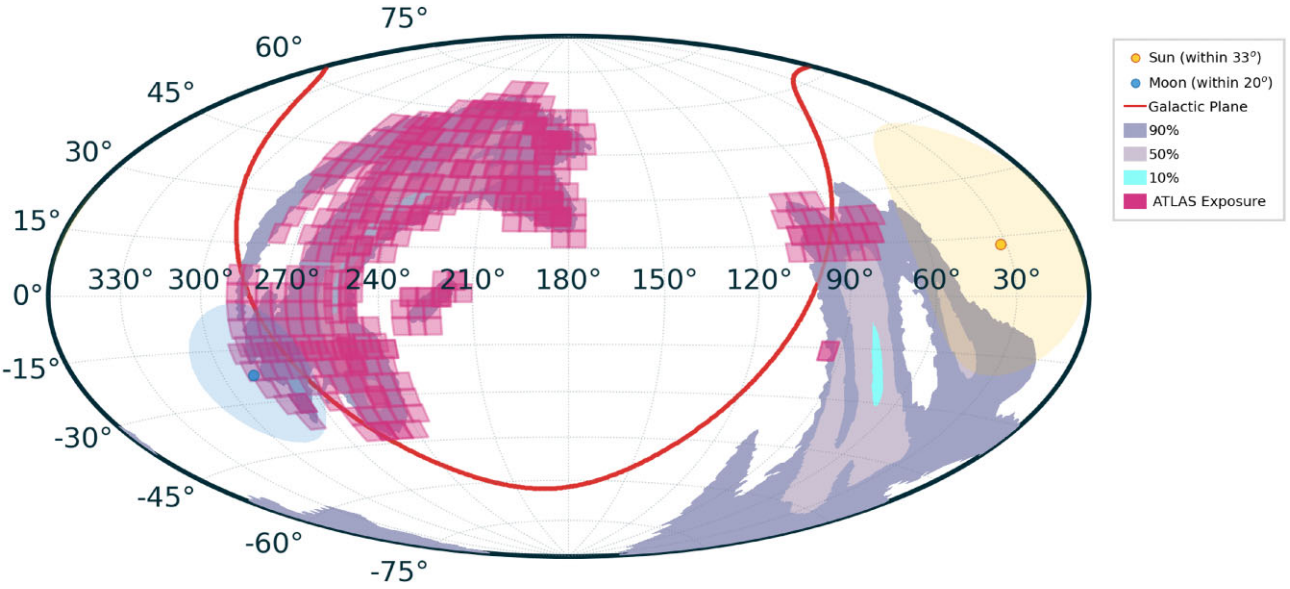

Figure 2. The ATLAS coverage over the first three nights of observation starting 0.8 h after the detection of GW190425. We used the `bayestar.fits` skymap to define our pointings at the time, but the map above shows the final GWTC-2 skymap as released on GraceDB. The cumulative probability covered at this stage was 41.6 per cent.

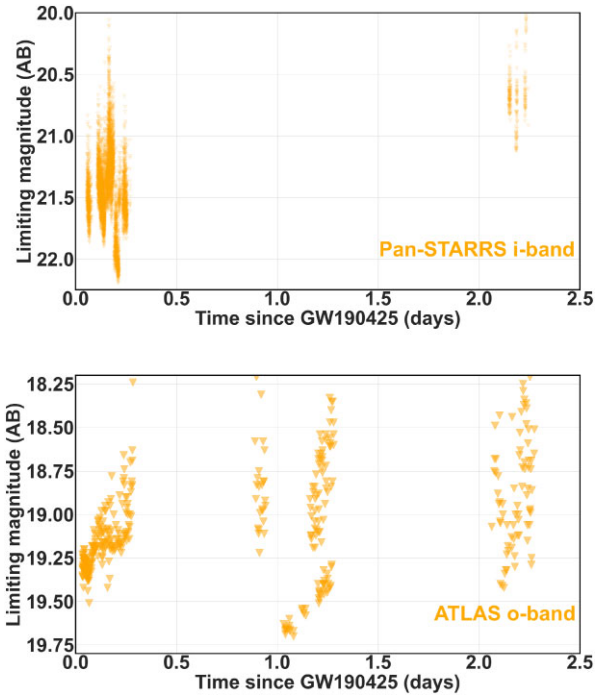

Figure 3. Illustration of the limiting magnitudes of PS1 i_{P1}-band (top) and ATLAS o-band imaging (bottom) of images that fell within the 90 per cent probability of the skymap `gw190425z_skymap.multiorder.fits` within the first 2.5 d. The zero time is set to the GW detection time MJD 58598.34589. Each PS1 point represents the 3.5σ limiting magnitude in a single skycell of the processed GPC1 frame with exposure times of 45 s. The ATLAS points represent the 5σ limiting magnitudes in a single full-frame ATLAS camera footprint of 30 s.

of the skymap within the first hour of the preliminary notice. During the first night, ATLAS covered 2799 deg^2 of the 90 per cent credible region of the GWTC-2 skymap and covered a sky region totalling 32.7 per cent of the probability area. By the third night of observing, this was incremented to 4560 deg^2 and 41.6 per cent. The ATLAS coverage of the skymap is presented in Fig. 2 and the 5σ limiting magnitudes of the individual exposures are illustrated in Fig. 3. The median and standard deviation of the limiting magnitudes are $o > 19.2 \pm 0.3$.

In McBrien et al. (2019), we flagged 25 transients but all had flux detections before the GW190425 detection time. They were either already known transients, or we had detected flux in our own forced photometry in images taken before the merger. No further convincing counterpart candidates were found brighter than $o \sim 19.5$, which were plausibly associated with a galaxy within 100–200 Mpc (i.e. less than 50 kpc separation). We reported five marginal candidates and noted that they required independent confirmation (McBrien et al. 2019), but all five were not recovered by other surveys and therefore were likely noise artefacts (e.g. Nicholl et al. 2019a).

In the context of FRB 20190425A and its most likely host galaxy UGC 10667, we covered the position of this galaxy with ATLAS within 6.9 h after the GW signal. A single 30 s exposure covered the coordinates of UGC 10667 (the quad was not completed at this sky position) and no transient flux is observed to a limiting magnitude of $o > 18.2$ (this was one of the poorer images on the night of 58598).

ATLAS also covered this position at +1.23 d after GW190425 and this time the 4 × 30 o-quad was completed in good conditions. The four separate difference image frames were co-added and no transient is visible within several arcminutes of UGC 10667 to a 3.5σ limiting magnitude of $o > 20.6$. A summary of epoch and observations is given in Table 1.

2.3 Zwicky Transient Facility observations and public data of UGC 10667

The ZTF observed the skymap in some of its public survey modes as described in Coughlin et al. (2019). No transient source is found within 30 arcsec of UGC 10667 in the public stream

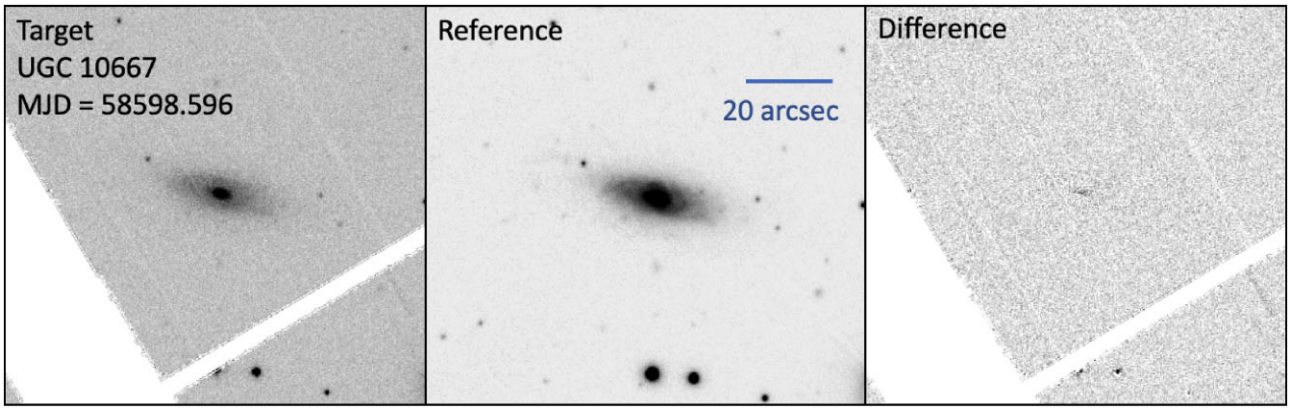

Figure 4. The PS1 images and difference images of the galaxy UGC 10667 from MJD = 58598.5957604. This i_{P1}-band image was taken 6.0 h after GW190425 merger time and 3.5 h after FRB 20190425A. As discussed in Section 2.1, the excess flux at the core of the galaxy is either a difference image residual or low-level AGN activity and there is no evidence of a transient source to typical depths of $i_{P1} > 21.6$ (north up and east left).

ingested by the Lasair broker[4] (Smith et al. 2019a). The ZTF survey (Bellm et al. 2019) allows forced photometry to be run at any position in the public data and the images to be requested (Masci et al. 2023). We forced photometry at five positions at and around UGC 10667 on three nights after the time of GW190425 (58598.414–58600.393) and inspected the difference images. No source was detected apart from what appears to be a difference image residual at the core of UGC 10667 on MJD 58599.397, similar to the PS1 residual in Fig. 4. The 3.5σ limits are listed in Table 1.

3 CONSTRAINTS ON KILONOVA EMISSION

The general constraints on kilonova emission across the sky area covered jointly by PS and ATLAS are inconclusive, given that we covered 24.9 per cent ($i_{P1} > 21.3 \pm 0.3$) and 41.2 per cent ($o \gtrsim 19.0$) integrated probability, respectively. At the estimated distance of GW190425 of $D_L = 159^{+69}_{-72}$ Mpc (Abbott et al. 2020), the PS1 data correspond to absolute magnitude limits of $M_i \gtrsim -14.7^{-0.9}_{+1.3}$, assuming negligible extinction and combining the standard deviation of the limits with the distance uncertainty in quadrature. For ATLAS, the observational constraints of $o > 19.2 \pm 0.3$ correspond to absolute magnitudes of $M_o \gtrsim -16.8^{-0.9}_{+1.3}$.

The ZTF covered 46 per cent of the initial skymap and 21 per cent of the final skymap to magnitudes $g, r \sim 21$ (Coughlin et al. 2019). At the distance of $D_L = 141 \pm 10$ Mpc, there are plausible models of kilonova emission (calculated with varying ejecta masses and electron fractions) that would go undetected at the limits of PS, ZTF, and ATLAS (e.g. Bulla 2019; Nicholl et al. 2021).

Other searches for counterparts were similar to, or less constraining than, the PS + ATLAS + ZTF combination in their coverage of the skymap (e.g. Hosseinzadeh et al. 2019; Lundquist et al. 2019; Antier et al. 2020; Gompertz et al. 2020). There is little quantitative and meaningful limit that can be placed on the emission of a kilonova from this single event given the observing constraints.

3.1 Constraints on kilonova emission specifically in UGC 10667

We can directly and quantitatively assess the plausibility of optical emission from GW190425 if FRB 20190425A is associated with the GW emission and if UGC 10667 is the host galaxy as proposed by Moroianu et al. (2023) and Panther et al. (2023).

To assess the significance of our non-detections of any optical emission from UGC 10667, we compare to a range of representative kilonova light-curve models generated using MOSFIT (Villar et al. 2017; Guillochon et al. 2018; Nicholl et al. 2021); these are shown in Fig. 5. Models are calculated in the ATLAS and PS filters and at the distance of UGC 10667, adopting also the foreground reddening from NED. The simplest comparison is with the well-sampled, nearby kilonova AT2017gfo (from GW 170817). For this, we use the best-fitting parameters from Nicholl et al. (2021) changing only the distance and extinction. The reader is referred to Nicholl et al. (2021) for details of the model assumptions. The PS 6.0 h limit and the ATLAS limit at +1.22 d both disfavour kilonova emission similar to that predicted for the GW170817 model (which matches the AT2017gfo data well).

The GW190425 signal favoured a more massive merger than GW170817, and indeed more massive than any known Galactic NS binary, with a chirp mass $\mathcal{M} = 1.44\,M_\odot$ (total mass $\approx 3.4\,M_\odot$). This suggests that a kilonova model calculated specifically for GW190425 may be more appropriate. We use a BNS-informed model from Nicholl et al. (2021), with a narrow Gaussian prior on $\mathcal{M}$ and a flat prior on the mass ratio $0.8 \leq q \leq 1$. We also marginalize over uncertainties in the fraction of the remnant disc ejected ($0.1 \leq \epsilon_{\rm disc} \leq 0.5$), the fraction of lanthanide-poor ejecta from dynamical, rather than magnetic, processes ($0.5 \leq \alpha \leq 1$), and the fraction of polar ejecta heated by a GRB jet ($0 \leq \zeta_{\rm sh} \leq 0.5$). The median light curve for GW190425 is $\approx$0.7–1 mag fainter at peak than GW170817 (Nicholl et al. 2021), though the uncertainties in parameters unconstrained by the GW signal result in a 90 per cent credible range spanning roughly ± 1 mag around the median. The early PS1 data point rules out the median model and excludes $\approx$75 per cent of our model realizations. However, we note that since the models include several parameters without physically informed priors, this is not equivalent to ruling out a kilonova at 75 per cent confidence.

For these simplest GW170817 and GW190425 models, we have assumed a maximum stable NS mass $M_{\rm TOV} = 2.17\,M_\odot$ (Margalit & Metzger 2017; Nicholl et al. 2021). However, the time delay between the GW and FRB signals favours a substantially larger $M_{\rm TOV}$ (Moroianu et al. 2023). A remnant NS in uniform rotation near break-up velocity is stable against collapse if its gravitational mass $M_{\rm rem} > 1.2 M_{\rm TOV}$. Thus, to avoid prompt collapse of the rather massive remnant $M_{\rm rem} \approx 3.2\,M_\odot$ (Abbott et al. 2020), an association between

[4] https://lasair-ztf.lsst.ac.uk

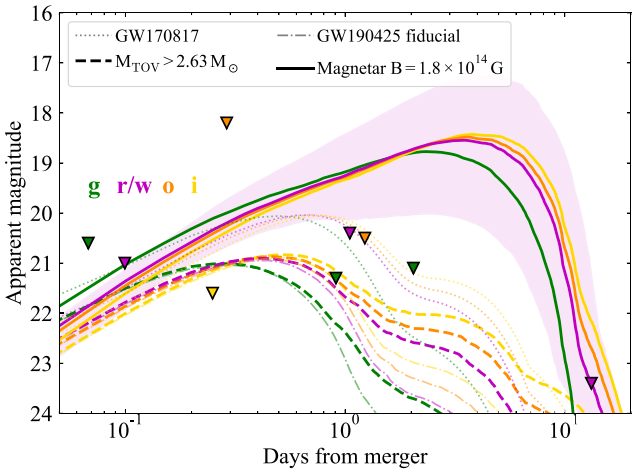

Figure 5. The upper limits measured by PS1, ATLAS, and ZTF in images taken of UGC 10667 are plotted as inverted triangles. The w_{P1} filter is very close to r band and is plotted in the same style. Three models of kilonova emission are plotted. The dotted and dashed lines are radioactively powered kilonova emissions of GW170817 (AT2017gfo) and the fiducial model of ejecta mass of GW190425 estimated by Nicholl et al. (2021), see Section 3.1. A more luminous model with emission enhanced by a magnetar as described in Section 3.2 is the solid line with model uncertainty regions. The models are calculated assuming a distance to UGC 10667 or UGC 10667 and the Milky Way foreground extinction as discussed in the text.

the GW and FRB signals requires $M_{TOV} > 2.6\,M_\odot$ (Moroianu et al. 2023). The authors also note that if the FRB results from the collapse of the remnant to a black hole (i.e. the remnant is not unstable indefinitely), we also have $M_{TOV} < 3.1\,M_\odot$. Marginalizing over this uncertainty in M_{TOV}, we find a light curve that looks essentially unchanged during the first ∼1 d (compared to the fiducial set of models with M_{TOV} set at 2.17 $M_\odot$) but is brighter by 1–2 mag during the next ∼week. This is the phase when the intermediate opacity disc wind ejecta are expected to dominate the observed emission, and the increase in luminosity with M_{TOV} results from the more massive disc wind from a longer lived remnant. These are plotted in Fig. 5, but the data we have are not constraining at the epochs that each set of models diverge.

3.2 Magnetar spin-down emission

If the link between GW190425 and FRB 20190425A were veracious and the physical picture is a supramassive (rotationally supported) NS remnant subsequently collapsing into a black hole after 2.5 h, the remnant must lose its rotational energy on this time-scale. Merger remnants are expected to be rotating near break-up (Radice et al. 2018), with $P \simeq 0.7$ ms. For remnants with $M_{TOV} < M_{rem} < 1.2 M_{TOV}$, the NS initially survives due to centrifugal support, and collapses once this is lost. Spin-down can occur through GW emission if the remnant has a quadrupole moment. However, we may expect that rotational energy loss is dominated by magnetic spin-down, particularly since the merger product is expected to have a strong magnetic field exceeding 10^{15} to 10^{16} G (Price & Rosswog 2006; Zrake & MacFadyen 2013; Kiuchi et al. 2023 – and assuming that the field is dominated by an ordered dipole; Dall'Osso, Shore & Stella 2009). Spinning down through dipole emission on a time-scale of 2.5 h requires only a modest $B \sim$ few $\times\ 10^{14}$ G (Moroianu et al. 2023).

The rotational energy extracted from the remnant can greatly enhance the kilonova luminosity (e.g. Yu, Zhang & Gao 2013; Gao et al. 2015; Fong et al. 2021; Sarin et al. 2022). Metzger (2019) provides an analytical model for the luminosity resulting from dipole spin-down in an NS merger remnant, and show that it can boost the optical emission very significantly, by up to ≈4 mag. We refer the reader to that work for details, but in brief this model takes into account the typical dipole spin-down formula for the evolution of the spin period and magnetar luminosity often applied to supernova remnants (e.g. Kasen & Bildsten 2010; Woosley 2010), and modifies it by a thermalization efficiency (close to unity at early times) and the energy removed by electron–positron pair creation at late times (Metzger & Piro 2014; Kasen, Metzger & Bildsten 2016). The input luminosity goes to zero as soon as the remnant collapses.

We have created a MOSFIT module to calculate magnetar-powered kilonova light curves using this framework. We assume a thermalization efficiency $\epsilon_{th} = 1$, an albedo of 0.5 for the pair cascade, and a pair multiplicity of 0.1 (as formulated in Metzger 2019). The resulting energy injected by the magnetar as it spins down is converted to an output optical luminosity using the usual Arnett (1982) model employed by MOSFIT. We have verified that this produces light curves in very good agreement with Metzger (2019). We fix the initial spin period at 0.7 ms (i.e. maximal spin), as expected from simulations. As the magnetar spins down, we compute the rotational energy at the time of collapse to a black hole following Margalit & Metzger (2017). The energy available to power the transient is the difference between the initial rotational energy and that at collapse.

In the case of FRB 20190425A, we fix $B = 1.8 \times 10^{14}$ G to give the appropriate time to collapse (Moroianu et al. 2023), resulting in no additional free parameters compared to the radioactive kilonova models. We marginalize over the chirp mass, mass ratio, and ejecta parameters with the same priors as before. This produces a luminous light curve, at all times brighter than the other models, and peaking later at ∼19 mag around 5–7 d after merger. The median model is strongly disfavoured by our PS and ATLAS observations of UGC 10667. Furthermore, in this case the credible range of the models does not overlap with our observational limits. More recent calculations of magnetar-boosted kilonovae from long-lived supramassive NSs also result in fluxes more than 10 to 100 times brighter than AT2017gfo (Wang, Beniamini & Giannios 2023). These are also inconsistent with our optical limits.

We return to the question of what this can tell us about the plausibility of the GW190425 and FRB 20190425A connection. If the FRB–GW connection were true, *and* if the merger did occur in UGC 10667, then we can exclude, with high confidence, that the merger produced a supramassive NS, spinning down by dipole emission on a time-scale of hours. The working model to produce FRB 20190425A from a BNS merger, as proposed by Moroianu et al. (2023), is that of a supramassive NS that is highly magnetized (Falcke & Rezzolla 2014; Zhang 2014). Hence, the lack of detected optical emission disfavours, but does not disprove, the FRB–GW link. Were such an FRB-producing remnant formed, then we have shown that it would likely have produced detectable optical emission. Bhardwaj et al. (2023a) propose that the FRB–GW association is unlikely as they find that a very low ejecta mass is required in order for the 400 MHz flux to propagate through the material ejected in the merger and that the viewing angle requirements from the FRB and GW data are inconsistent.

4 CONCLUSIONS

We promptly observed the LIGO–Virgo–KAGRA skymap of the BNS merger event GW190425 with PS and ATLAS beginning several hours after the merger event. With PS1, we managed to cover a total integrated probability area of 24.9 per cent (to limiting magnitudes of $i_{\rm P1} > 21.3 \pm 0.3$) over the first 3 d, and with ATLAS, we covered 41.2 per cent ($o > 19.2 \pm 0.3$). These correspond to absolute magnitudes of $M_i \gtrsim -14.7^{-0.9}_{+1.3}$ and $M_o \gtrsim -16.8^{-0.9}_{+1.3}$ (assuming negligible extinction) with the errors dominated by the uncertainty in the distance to GW190425. The physical limits on an electromagnetic counterpart to GW190425 are not strong, given that approximately half the skymap was unobservable due to solar conjunction – a problem that affected all wide-field searches for optical counterparts. However, they do show the joint capability of the ATLAS and PS systems for GW follow-up, particularly as ATLAS is now a four-unit system (and all-sky) and PS now is a twin facility on Haleakala.

A recently proposed connection between GW190425 and FRB 20190425A has emerged with a temporal and spatial coincidence found by Moroianu et al. (2023). If this association were to be physically true, then it implies that a supramassive, rapidly rotating, and magnetized NS was formed for at least a few hours after BNS merger (the GW and FRB signals were separated by 2.5 h). FRB 20190425A has been pinpointed to a most probable host galaxy, UGC 10667, which is at a compatible redshift with the distance to GW190425 (Moroianu et al. 2023; Panther et al. 2023). With PS and ATLAS, we observed this host galaxy within a few hours of the FRB and GW signals. No optical emission was found. We calculated samples of kilonova light curves with ejecta masses and radioactive heating based on the data from AT2017gfo and the physical parameters inferred from the GW data of GW190425 (Nicholl et al. 2021). The PS limiting magnitude of $i_{\rm P1} > 21.6$ at $+0.25$ d after GW190425 merger time precludes an AT2017gfo type of kilonova and marginally disfavours a fiducial kilonova model based on the GW190425 data.

The magnetized, rotating NS required to explain the FRB emission has a magnetic field of $B \sim 1.8 \times 10^{14}$ G, which would result in an enhancement of the kilonova luminosity by magnetar powering. We calculate such models by fixing the magnetic field to that required by the FRB and marginalizing over chirp mass, mass ratio, and ejecta parameters. The rather luminous optical light curves are all ruled out by the limits from PS1 and ATLAS within the first $+1.2$ d from merger. This excludes a supramassive NS, spinning down by dipole emission on a time-scale of hours. The lack of detected optical emission disfavours, but does not disprove, the FRB–GW link. If such an FRB–GW link were proven in the future (Moroianu et al. 2023), then the FRB sky localization and potential for immediate identification of a host galaxy (Panther et al. 2023) would be an extremely promising route to advance multimessenger astronomy and further such coincidences should be searched for.

ACKNOWLEDGEMENTS

Pan-STARRS is primarily funded to search for near-Earth asteroids through NASA grants NNX08AR22G and NNX14AM74G. The Pan-STARRS science products for LIGO–Virgo follow-up were made possible through the contributions of the University of Hawai'i Institute for Astronomy and the Queen's University Belfast. The Pan-STARRS1 sky surveys have been made possible through contributions by the Institute for Astronomy, the University of Hawai'i, the Pan-STARRS Project Office, the Max Planck Society and its participating institutes, the Max Planck Institute for Astronomy, Heidelberg and the Max Planck Institute for Extraterrestrial Physics, Garching, the Johns Hopkins University, Durham University, the University of Edinburgh, the Queen's University Belfast, the Harvard–Smithsonian Center for Astrophysics, the Las Cumbres Observatory Global Telescope Network Incorporated, the National Central University of Taiwan, the Space Telescope Science Institute, and the National Aeronautics and Space Administration under Grant No. NNX08AR22G issued through the Planetary Science Division of the NASA Science Mission Directorate, the National Science Foundation Grant No. AST-1238877, the University of Maryland, Eotvos Lorand University (ELTE), and the Los Alamos National Laboratory.

ATLAS is primarily funded to search for near-Earth asteroids through NASA grants NN12AR55G, 80NSSC18K0284, and 80NSSC18K1575; by-products of the NEO search include images and catalogues from the survey area. The ATLAS science products have been made possible through the contributions of the University of Hawai'i Institute for Astronomy, the Queen's University Belfast, the Space Telescope Science Institute, and the South African Astronomical Observatory.

Lasair is supported by the UKRI Science and Technology Facilities Council and is a collaboration between the University of Edinburgh (grant ST/N002512/1) and Queen's University Belfast (grant ST/N002520/1) within the LSST:UK Science Consortium. ZTF is supported by National Science Foundation grant AST-1440341 and a collaboration including Caltech, IPAC, the Weizmann Institute for Science, the Oskar Klein Center at Stockholm University, the University of Maryland, the University of Washington, Deutsches Elektronen-Synchrotron and Humboldt University, Los Alamos National Laboratories, the TANGO Consortium of Taiwan, the University of Wisconsin at Milwaukee, and Lawrence Berkeley National Laboratories. Operations are conducted by COO, IPAC, and UW. This research has made use of 'Aladin sky atlas' developed at CDS, Strasbourg Observatory, France.

SJS, SS, LS, KWS, and DRY acknowledge UKRI STFC grants ST/X006506/1, ST/T000198/1, ST/S006109/1, and ST/X001253/1. MN, AA and SS and were supported by the European Research Council (ERC) under the European Union's Horizon 2020 research and innovation programme (Grant Agreement No. 948381). MN also acknowledges UK Space Agency Grant No. ST/Y000692/1. T-WC acknowledges the Yushan Young Fellow Program by the Ministry of Education, Taiwan for the financial support. LS acknowledges support by the European Research Council (ERC) under the European Union's Horizon 2020 research and innovation programme (ERC Advanced Grant KILONOVA No. 885281) and support by Deutsche Forschungsgemeinschaft (DFG, German Research Foundation) – Project ID 279384907 – SFB 1245 and MA 4248/3-1. This work was funded by ANID, Millennium Science Initiative, ICN12_009. CWS is grateful for support from Harvard University. This research has made use of the NED, which is operated by the Jet Propulsion Laboratory, California Institute of Technology, under contract with the National Aeronautics and Space Administration. For the purpose of open access, a Creative Commons Attribution (CC BY 4.0) licence will apply to any Author Accepted Manuscript version arising.

DATA AVAILABILITY

The data tables for the ATLAS and PS exposures (to produce Figs 1–3) are available as supplementary files (csv tabular format). The code for the models to produce Fig. 5 is available on the MOSFIT (https://github.com/guillochon/MOSFiT).

REFERENCES

Abbott B. P. et al., 2017a, Phys. Rev. Lett., 119, 161101
Abbott B. P. et al., 2017b, ApJ, 848, L12
Abbott B. P. et al., 2017c, ApJ, 848, L13
Abbott B. P. et al., 2020, ApJ, 892, L3
Abbott R. et al., 2021, Phys. Rev. X, 11, 021053
Abbott R. et al., 2023, ApJ, 955, 155
Aggarwal K., Budavári T., Deller A. T., Eftekhari T., James C. W., Prochaska J. X., Tendulkar S. P., 2021, ApJ, 911, 95
Albareti F. D. et al., 2017, ApJS, 233, 25
Alexander K. D. et al., 2017, ApJ, 848, L21
Andreoni I. et al., 2017, Publ. Astron. Soc. Aust., 34, e069
Antier S. et al., 2020, MNRAS, 497, 5518
Arcavi I. et al., 2017, Nature, 551, 64
Arnett W. D., 1982, ApJ, 253, 785
Bellm E. C. et al., 2019, PASP, 131, 018002
Bhardwaj M., Palmese A., Magaña Hernandez I., D'Emilio V., Morisaki S., 2023a, preprint (arXiv:2306.00948)
Bhardwaj M. et al., 2023b, preprint (arXiv:2310.10018)
Boersma O. M. et al., 2021, A&A, 650, A131
Bulla M., 2019, MNRAS, 489, 5037
Chambers K. C. et al., 2016, preprint (arXiv:1612.05560)
CHIME/FRB Collaboration, 2021, ApJS, 257, 59
Chornock R. et al., 2017, ApJ, 848, L19
Cooper A. J., Gupta O., Wadiasingh Z., Wijers R. A. M. J., Boersma O. M., Andreoni I., Rowlinson A., Gourdji K., 2023, MNRAS, 519, 3923
Coughlin M. W. et al., 2019, ApJ, 885, L19
Coulter D. A. et al., 2017, Science, 358, 1556
Cowperthwaite P. S. et al., 2017, ApJ, 848, L17
Dall'Osso S., Shore S. N., Stella L., 2009, MNRAS, 398, 1869
Dimitriadis G. et al., 2019, GCN Circ., 24358, 1
Drout M. R. et al., 2017, Science, 358, 1570
Evans P. A. et al., 2017, Science, 358, 1565
Falcke H., Rezzolla L., 2014, A&A, 562, A137
Fong W. et al., 2021, ApJ, 906, 127
Fong W.-f. et al., 2022, ApJ, 940, 56
Gao H., Ding X., Wu X.-F., Dai Z.-G., Zhang B., 2015, ApJ, 807, 163
Gillanders J. H. et al., 2023,. preprint (arXiv:2308.00633)
Gompertz B. P. et al., 2020, MNRAS, 497, 726
Guillochon J., Nicholl M., Villar V. A., Mockler B., Narayan G., Mandel K. S., Berger E., Williams P. K. G., 2018, ApJS, 236, 6
Haggard D., Nynka M., Ruan J. J., Kalogera V., Cenko S. B., Evans P., Kennea J. A., 2017, ApJ, 848, L25
Hallinan G. et al., 2017, Science, 358, 1579
Hosseinzadeh G. et al., 2019, ApJ, 880, L4
Jonker P. et al., 2019, GCN Circ., 24221, 1
Kasen D., Bildsten L., 2010, ApJ, 717, 245
Kasen D., Metzger B. D., Bildsten L., 2016, ApJ, 821, 36
Kasliwal M. M. et al., 2017, Science, 358, 1559
Kilpatrick C. D. et al., 2017, Science, 358, 1583
Kiuchi K., Reboul-Salze A., Shibata M., Sekiguchi Y., 2023, preprint (arXiv:2306.15721)
Levan A. et al., 2023, Nature, preprint (arXiv:2307.02098)
LIGO Scientific Collaboration, The Virgo Collaboration, 2019a, GCN Circ., 24168, 1
LIGO Scientific Collaboration, The Virgo Collaboration, 2019b, GW190425 Data Set, version 1, doi:10.7935/ggb8-1v94, last accessed on 1 September 2023.
Lipunov V. M. et al., 2017, ApJ, 850, L1
Lundquist M. J. et al., 2019, ApJ, 881, L26
McBrien O. et al., 2019, GCN Circ., 24197, 1
McCully C. et al., 2017, ApJ, 848, L32
McCully C. et al., 2019, GCN Circ., 24295, 1
Magnier E. A. et al., 2020a, ApJS, 251, 3
Magnier E. A. et al., 2020b, ApJS, 251, 5
Magnier E. A. et al., 2020c, ApJS, 251, 6
Margalit B., Metzger B. D., 2017, ApJ, 850, L19
Margutti R. et al., 2017, ApJ, 848, L20
Masci F. J. et al., 2023, preprint (arXiv:2305.16279)
Metzger B. D., 2019, Living Rev. Relativ., 23, 1
Metzger B. D., Piro A. L., 2014, MNRAS, 439, 3916
Moroianu A., Wen L., James C. W., Ai S., Kovalam M., Panther F. H., Zhang B., 2023, Nat. Astron., 7, 579
Morokuma T. et al., 2019, GCN Circ., 24230, 1
Nicholl M. et al., 2017, ApJ, 848, L18
Nicholl M. et al., 2019a, GCN Circ., 24211, 1
Nicholl M. et al., 2019b, GCN Circ., 24217, 1
Nicholl M., Margalit B., Schmidt P., Smith G. P., Ridley E. J., Nuttall J., 2021, MNRAS, 505, 3016
Panther F. H. et al., 2023, MNRAS, 519, 2235
Paterson K. et al., 2021, ApJ, 912, 128
Pian E. et al., 2017, Nature, 551, 67
Planck Collaboration XIII, 2016, A&A, 594, A13
Price D. J., Rosswog S., 2006, Science, 312, 719
Radice D., Perego A., Bernuzzi S., Zhang B., 2018, MNRAS, 481, 3670
Ravi V., 2019, MNRAS, 482, 1966
Sarin N., Omand C. M. B., Margalit B., Jones D. I., 2022, MNRAS, 516, 4949
Schlafly E. F., Finkbeiner D. P., 2011, ApJ, 737, 103
Shappee B. J. et al., 2017, Science, 358, 1574
Singer L. P., Price L. R., 2016, Phys. Rev. D, 93, 024013
Smartt S. J. et al., 2016a, MNRAS, 462, 4094
Smartt S. J. et al., 2016b, ApJ, 827, L40
Smartt S. J. et al., 2017, Nature, 551, 75
Smith K. W. et al., 2019a, Res. Notes Am. Astron. Soc., 3, 26
Smith K. W. et al., 2019b, GCN Circ., 24210, 1
Smith K. W. et al., 2019c, GCN Circ., 24262, 1
Smith K. W. et al., 2020, PASP, 132, 085002
Soares-Santos M. et al., 2017, ApJ, 848, L16
Stalder B. et al., 2017, ApJ, 850, 149
Tanvir N. R. et al., 2017, ApJ, 848, L27
Tonry J. L. et al., 2012, ApJ, 745, 42
Tonry J. L. et al., 2018, PASP, 130, 064505
Totani T., 2013, PASJ, 65, L12
Troja E. et al., 2017, Nature, 551, 71
Utsumi Y. et al., 2017, PASJ, 69, 101
Valenti S. et al., 2017, ApJ, 848, L24
Villar V. A. et al., 2017, ApJ, 851, L21
Wang H., Beniamini P., Giannios D., 2023, MNRAS, 527, 5166
Waters C. Z. et al., 2020, ApJS, 251, 4
Woosley S. E., 2010, ApJ, 719, L204
Wright D. E. et al., 2015, MNRAS, 449, 451
Yang Y.-H. et al., 2023, preprint (arXiv:2308.00638)
Yu Y.-W., Zhang B., Gao H., 2013, ApJ, 776, L40
Zhang B., 2014, ApJ, 780, L21
Zrake J., MacFadyen A. I., 2013, ApJ, 769, L29

SUPPORTING INFORMATION

Supplementary data are available at *MNRAS* online.

GW190425_atlas_exposures.csv
GW190425_ps_exposures.csv
Please note: Oxford University Press is not responsible for the content or functionality of any supporting materials supplied by the authors. Any queries (other than missing material) should be directed to the corresponding author for the article.

This paper has been typeset from a TEX/LATEX file prepared by the author.